Performance Evaluation of Cross-Polarized Antenna Selection over 2 GHz Measurement-Based Channel Models

Nishimoto, H.; Taira, A.; Kubo, H.; Pun, M-O; Annavajjala, R.; Molisch, A.F.

Abstract

In a multiple-input multiple-output (MIMO) system, cross-polarized antenna selection yields significant reduction in cost and hardware size. However, actual benefits of the technique are dependent on the propagation characteristics including channel polarization. To accurately characterize the target 2 GHz-band MIMO channels, the authors conduct 2 GHz cross-polarized channel measurement campaigns. Based on the measured data, novel channel models specifically for the 2 GHz bands are established. In addition, we evaluate the performance improvement obtained with cross-polarized antenna selection using the channel models. Simulation results reveal that antenna selection is particularly useful in the low SNR regime, and that the system capacity at cell edges can be increased up to 13%.

Performance Evaluation of Cross-Polarized Antenna Selection over 2 GHz Measurement-Based Channel Models

H. Nishimoto, A. Taira, H. Kubo
Information Technology R&D Center, Mitsubishi Electric Corp.
5-1-1 Ofuna, Kamakura, Kanagawa 247-8501, Japan

M.-O. Pun, R. Annavajjala, and A.F. Molisch
Mitsubishi Electric Research Labs. (MERL)
201 Broadway, Cambridge, MA 02139, USA

Abstract—**In a multiple-input multiple-output (MIMO) system, cross-polarized antenna selection yields significant reduction in cost and hardware size. However, actual benefits of the technique are dependent on the propagation characteristics including channel polarization. To accurately characterize the target 2 GHz-band MIMO channels, the authors conduct 2 GHz cross-polarized channel measurement campaigns. Based on the measured data, novel channel models specifically for the 2 GHz bands are established. In addition, we evaluate the performance improvement obtained with cross-polarized antenna selection using the channel models. Simulation results reveal that antenna selection is particularly useful in the low SNR regime, and that the system capacity at cell edges can be increased up to 13%.**

I. INTRODUCTION

Multiple-input multiple-output (MIMO) technology is a promising technique to achieve higher capacity in wireless communications. However, MIMO transmitter/receiver suffers from higher cost and larger hardware size because it requires multiple antennas and radio frequency (RF) circuits.

Antenna selection enables us to overcome this obstacle because the required number of RF circuits can be reduced to the number of selected active antennas. Also, cross-polarized antennas can be implemented in a much confined space compared to identically polarized antennas. A cross-polarized antenna selection scheme incorporating these two techniques therefore is expected to lead to significant reduction in cost and hardware size without sacrificing the advantages of the MIMO systems.

On the other hand, effective benefits of these techniques are dependent on the propagation environment. Channel characterization including polarization in actual environments is particularly of importance. WINNER [1], which is a channel model extensively used for examining MIMO systems, takes into account polarization. Since it supports 2–6 GHz bands, its parameters were not specifically derived for the 2 GHz bands, which are currently employed in various cellular systems. In particular, cross polarization discrimination (XPD), which is well-known as a key factor determining the cross-polarized channel characteristic and has been extensively examined in the past channel measurement campaigns [2], should be verified for fair evaluation of the cross-polarized antenna selection scheme.

In this work, to accurately characterize the 2 GHz-band MIMO channels, the authors conduct 2 GHz cross-polarized channel measurement campaigns. Based on the measured data, novel channel models specific to 2 GHz bands are established. Finally, we evaluate the effect of the cross-polarized antenna selection technique over the channel models.

Hereafter, we define N_{tx} and N_{rx} as the number of transmit (TX) antennas and the number of receive (RX) anten-
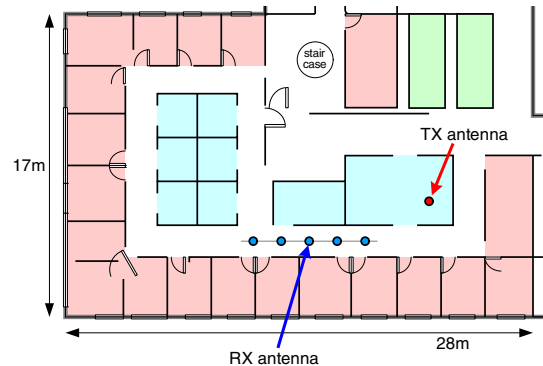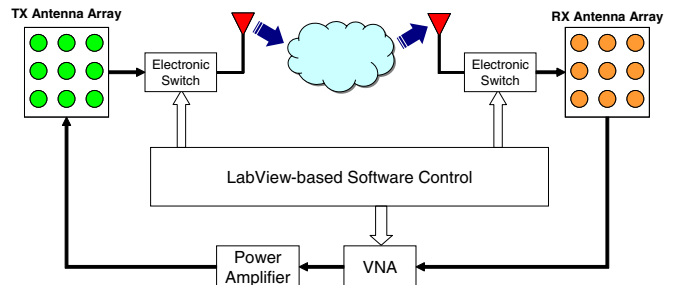

Fig. 1. Measurement site (Scenario B).

Fig. 2. Measurement block diagram.

nas, respectively. Thus, a MIMO channel is expressed by an $N_{rx} \times N_{tx}$ matrix. Also, V and H denote vertical and horizontal polarizations, respectively.

II. CHANNEL MEASUREMENT

A. Channel Measurement Setup

MIMO channel measurement campaigns were conducted in Cambridge, MA. Four scenarios were considered in the measurement: (A) office line-of-sight (LOS), (B) office non-LOS (NLOS), (C) residential indoor-to-indoor NLOS, and (D) residential indoor-to-outdoor NLOS. For example, we show a top view of measurement layout in Scenario B in Fig. 1. Scenarios A and B were measured in generic office environments, and Scenarios C and D were realized in a wooden free-standing house. We used a 2 GHz band with 200 MHz bandwidth.

Figure 2 illustrates the block diagram for channel measurements. Data was collected at multiple locations by moving the receiver away from a fixed transmitter. Furthermore, to facilitate MIMO channel modeling, measurements are taken

at each receiver location by moving both the transmitter and receiver locally in a 3×3 grid whose minimum distance between any two points is half a wavelength (i.e. about 6.5 cm). We employed dipole antennas designed for omni-directional characteristics. All of the antennas had return loss less than -10 dB in the measurement band. Since we are interested in the channel polarization characteristics, measurements were taken by using vertically and horizontally polarized antennas sequentially at each receiver location while the TX antenna was vertically polarized. As a result, total $9 \times 9 \times 2 = 162$ data sets were recorded by the vector network analyzer (VNA) at each location. TX and RX antennas were set at a height of 1.5 m. For each transmitter-receiver pair, and for each of the two polarizations, we have taken five VNA snapshots. Assuming that the channel remains stationary within the snapshots, we have averaged the snapshots to reduce the noise impairment. The losses incurred by the cables used at the transmitter and the receiver were accounted in our calibration procedure. We have also separately measured the antenna patterns of the transmitter and the receiver antennas over the operating frequency band. The measured data, along with the calibration data and the antenna patterns, was then processed off-line to extract channel model parameters.

B. Channel Modeling Approach

It is well recognized that a good channel model should be concise and accurate. However, in contrast to conventional single-input single-output (SISO) channel models, it requires many more parameters to accurately characterize the spatial information of MIMO channels. Thus inspired, various approaches have been proposed in the literature to model MIMO channels. Generally speaking, the existing approaches can be classified into two categories, namely physical and non-physical approaches. In non-physical approaches, the measured data is directly transformed to generate transfer matrices without exploiting the underlying physical interpretations. Despite its simplicity, the non-physical approach offers little insight into the channel characteristics. In contrast, the physical approach exploits the structure of MIMO channels under consideration. One of the modern physical approaches is the double-directional model that separates antenna- and channel-related information. Mathematically, a time-varying frequency-selective MIMO channel impulse response can be written as

$$\boldsymbol{H}(t, \tau) = \sum_{n=1}^{N_{\mathrm{mpc}}} \boldsymbol{H}_n(t, \tau) \delta(t - \tau_n(t)), \quad (1)$$

where N_{mpc} is the number of multipath components (MPC), and $\boldsymbol{H}_n$ and $\tau_n(t)$ are the time-varying MIMO channel component and delay of the n-th MPC respectively. In the double-directional channel models, the (i, j)-th element of $\boldsymbol{H}_n$, where $1 \leq i \leq N_{\mathrm{rx}}$ and $1 \leq j \leq N_{\mathrm{tx}}$, is modeled as

$$h_{n,i,j}(t, \tau) = \begin{bmatrix} F_{\mathrm{rx},i,V}(\phi_{\mathrm{rx},n}) \\ F_{\mathrm{rx},i,H}(\phi_{\mathrm{rx},n}) \end{bmatrix}^H \begin{bmatrix} \alpha_{n,VV} & \alpha_{n,VH} \\ \alpha_{n,HV} & \alpha_{n,HH} \end{bmatrix} \begin{bmatrix} F_{\mathrm{tx},j,V}(\phi_{\mathrm{tx},n}) \\ F_{\mathrm{tx},j,H}(\phi_{\mathrm{tx},n}) \end{bmatrix}, \quad (2)$$

where $F(\cdot)$ is the antenna response with $\phi_{\mathrm{rx},n}$ and $\phi_{\mathrm{tx},n}$ being the angle of arrival (AoA) and angle of departure (AoD) of the n-th MPC. Note that this antenna response includes the effects of mutual coupling and the specific location of the element, most importantly the direction-dependent phase shift that a signal undergoes on its way from the reference position of the TX (or RX) array to the actual location of the antenna element. Furthermore, the channel polarization characteristics
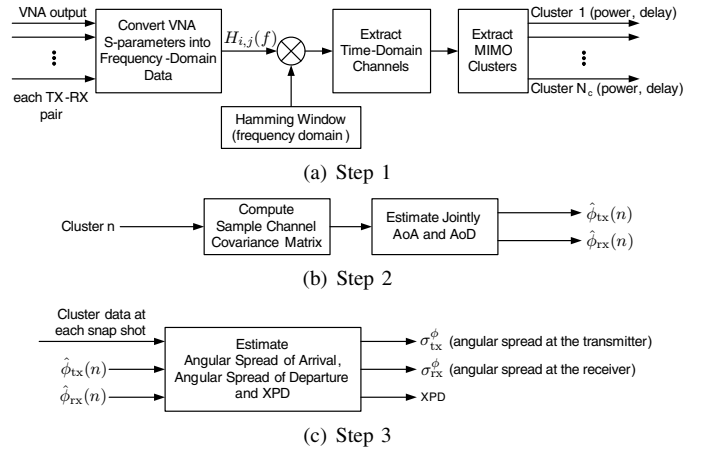

(a) Step 1

(b) Step 2

(c) Step 3

Fig. 3. Parameter extraction process.

are defined by the complex channel gains $\alpha_{n,VV}$, $\alpha_{n,VH}$, $\alpha_{n,HV}$, and $\alpha_{n,HH}$.

Modeling the parameters of a double-directional channel models can be done by either deterministic (such as ray-tracing) or stochastic (such as tapped-delay line) methods. While the deterministic model can provide highly accurate channel models by exploiting the geometric information of measurement environment, it suffers from prohibitive computational complexity and more importantly, it renders little insight for many applications because the characteristics highly depend on the specific environment. In contrast, the stochastic approach provides reasonably accurate channel models at affordable computational complexity. As a result, the stochastic approach has been widely adopted in most recent standards including WINNER, IEEE 802.11n and 3GPP SCM [1]. In the sequel, the tapped-delay line (TDL) approach will be employed in our models.

C. Parameter Extraction

Inspection of eq. (2) suggests that the TDL model is defined by AoA and AoD of each MPC in addition to parameters such as path loss and path delays. Furthermore, the XPD factor defined as $\left| \alpha_{n,VV}/\alpha_{n,HV} \right|$ also plays a critical role in the model. The following three steps are performed to extract these model parameters.

Step 1: First, the VNA output measured from each TX-RX antenna pair is normalized to calibration data and then converted from the frequency domain to the time domain via inverse Fourier transform. Note that a Hamming window is applied before inverse Fourier transform in order to suppress sidelobes of the time-domain data. Following the same definition in the WINNER channel models [1], we group the MPCs into groups, called "clusters" whose delays can be distinguished by inverse Fourier transform. In other words, we assume a regularly-spaced tapped delay line structure, and call each tap a "cluster." In our case, time resolution of each cluster corresponds to the inverse of the measurement bandwidth, namely $1/(200 \text{ MHz}) = 5$ ns. Assuming that there are N_c clusters of MPCs, we can extract the information of power and delay of each cluster. Repeating the same processes for data measured from each TX-RX pair, we can obtain the MIMO cluster information as shown in Fig. 3(a).

Step 2: Next, the sample channel correlation matrix of each MIMO cluster is derived before its AoA and AoD are estimated as shown in Fig. 3(b).

	Scenario			
	A	B	C	D
RMS Delay Spread (ns)	28.1	31.2	13.3	12.0
V-V TX Angular Spread (deg)	76.3	66.2	104.6	64.8
V-V RX Angular Spread (deg)	83.4	123.8	118.9	70.3
V-H TX Angular Spread (deg)	89.1	66.1	97.9	97.2
V-H RX Angular Spread (deg)	84.1	126.8	87.7	61.4
XPD (dB)	2.7	0.3	2.6	3.6

There are various techniques to derive AoA and AoD from the sample channel correlation matrix. In this work, we employed the following minimum variance method (MVM) (also well-known as Capon method [3]) due to its simplicity:

$$\left\{\hat{\phi}_{\text{tx}}(n), \hat{\phi}_{\text{rx}}(n)\right\} = \arg\max_{\phi_{\text{tx}}, \phi_{\text{rx}}} \frac{1}{\boldsymbol{a}^H\left(\phi_{\text{tx}}, \phi_{\text{rx}}\right) \boldsymbol{R}_n^{-1} \boldsymbol{a}\left(\phi_{\text{tx}}, \phi_{\text{rx}}\right)}, \quad (3)$$

where $\boldsymbol{a}\left(\phi_{\text{tx}}, \phi_{\text{rx}}\right)$ is the array response vector, and $\boldsymbol{R}_n$ is the sample channel correlation matrix of the n-th cluster after spatial smoothing preprocessing. We note that eq.(3) can also be used to search for more than one pair of angles by identifying the peaks of the MVM spectra.

Step 3: Finally, the estimated $\left\{\hat{\phi}_{\text{tx}}(n), \hat{\phi}_{\text{rx}}(n)\right\}$ are exploited to compute their angular spreads as well as the corresponding XPD. Figure 3(c) depicts the parameter extraction for AoA and AoD angular spreads along with XPD.

D. Polarized MIMO Channel Models

Table I shows some key model parameters derived from our measurement in the four scenarios. In addition, we realized Ricean K-factor of around 4 dB in Scenario A.

Here, we compare the obtained parameters with existing WINNER. The parameters should be comparable because the generic channel model we use is similar to the WINNER generic model (which in turn is derived from the 3GPP-SCM model). In WINNER office LOS (A1-LOS) and office NLOS (A1-NLOS) scenarios, reported XPD factors are 11 dB and 10 dB, respectively [1]. It is noticeable that the XPD factors in our measurement scenarios A (office LOS) and B (office NLOS) are different from those in WINNER. To validate the difference, we also performed additional measurement over a 5 GHz band with 100 MHz bandwidth in the same scenarios. By comparing our 5 GHz-band measurement results against those in WINNER, we confirmed that our channel models obtained with the WINNER setup match well with WINNER. An example of the derived XPD in Scenario B is shown in Fig. 4. Inspection of Fig. 4 reveals that the estimated XPD in the 5 GHz band is approximately Gaussian distributed with mean of about 8 dB, which is much higher than the result in the 2 GHz band, or 0.3 dB, and is close to that of WINNER. We say that radio propagation characteristics including polarization have frequency dependency even between 2 and 5 GHz bands [4], and that our results are in line with the WINNER by the 5 GHz band comparison. We therefore conclude that our established models are valid and have more suitability for 2 GHz-band systems than WINNER.

III. CROSS-POLARIZED ANTENNA SELECTION

A. Transmit Antenna Selection

In this section, we investigate the performance improvement using polarized antenna selection in downlink transmissions. In the paper, we deal with $N_{\text{tx}} = N_{\text{rx}} = 2$ cross-polarized MIMO systems. While we assume that a user terminal (UT)
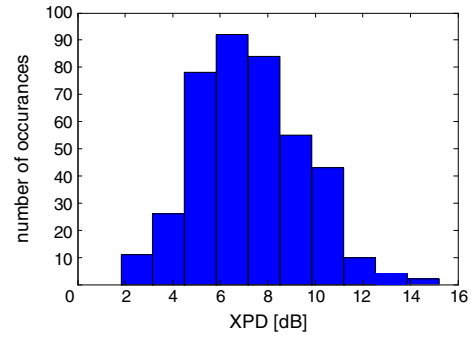

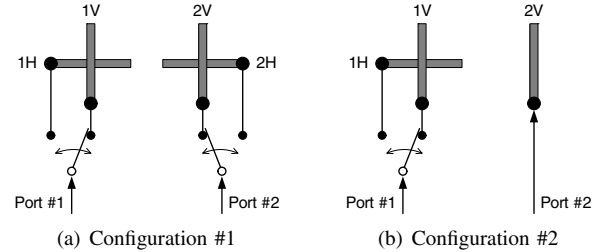Fig. 4. Estimated XPD in Scenario B using WINNER setup (5 GHz band).

(a) Configuration #1   (b) Configuration #2

Fig. 5. Two BS transmitter antenna configurations.

	1V-2H	1V-2V	1H-2V	1H-2H
Non-Antenna Selection (2 antennas)	—	—	○	—
Configuration #1 (4 antennas)	○	○	○	○
Configuration #2 (3 antennas)	—	○	○	—

is equipped with one pair of V-H cross-polarized antennas, two different antenna configurations are examined for a base station (BS) as shown in Fig. 5. More specifically, Configuration #1 is equipped with two pairs of V-H cross-polarized antennas and two antenna switches whereas Configuration #2 has only one pair of V-H cross-polarized antennas and one vertically polarized antenna. Clearly, Configuration #1 can support four antenna combinations (i.e. 1V-2H, 1V-2V, 1H-2V, 1H-2H) whereas Configuration #2 only two (i.e. 1V-2V and 1H-2V). For presentational convenience, the performance obtained with two cross-polarization antennas is referred to as the non-antenna selection (non-AS) performance and serves as the baseline in the sequel. Table II summarizes the available antenna combinations in different TX antenna configurations under consideration.

To facilitate antenna selection, the following mechanism has been specified for frequency-division duplex (FDD) systems to collect information of channel quality indicator (CQI), precoding matrix indicator (PMI) and rank indicator (RI) from UTs. For each available antenna combination, a BS sends out channel state information reference signals (CSI-RS) to its UTs in a subframe of 1 ms from the two chosen antennas. Upon receiving the RS, the UT evaluates the highest supportable data rate and the corresponding PMI and RI before returning the estimated information back to the BS in uplink [5]. It should be emphasized that about 8 ms delay is incurred between the instant a BS sends out RS and the instant it transmits data using the returned PMI. Considering a Doppler frequency of 6 Hz (i.e. a mobile speed of 3 km/hr at 2 GHz), the coherence time is only about 30 ms. As a result, the adverse impact of having more available antenna combinations is the reduction

of useful data transmission duration within the coherence time.

B. CQI Evaluation at UT

Next, we discuss the CQI evaluation procedures taken by the UT to obtain the optimal CQI/PMI/RI. For presentational simplicity, we concentrate our following discussions on one subcarrier. Furthermore, we assume that the UT has obtained perfect MIMO channel matrix estimation at that subcarrier, denoted by $\boldsymbol{H}$. Given the average signal-to-noise ratio (SNR) denoted by ρ, the MIMO channel capacity with water-filling power allocation is given by

$$C = \log_2 \det\left[\boldsymbol{I}_2 + \frac{\rho}{2}\boldsymbol{H}\boldsymbol{Q}\boldsymbol{H}^H\right] = \sum_{r=1}^{2}\left[\log_2 \mu\lambda_r\right]^+, \qquad (4)$$

where $\boldsymbol{Q}$ is the covariance matrix of optimally precoded and power-allocated TX signals with trace $(\boldsymbol{Q}) \le 2$ and

$$\sum_{r=1}^{2}\left[\mu - \frac{1}{\lambda_r}\right]^+ = \rho, \qquad (5)$$

with $\{\lambda_r; \lambda_1 \ge \lambda_2\}$ being the eigenvalues of $\boldsymbol{H}\boldsymbol{H}^H$ and

$$[x]^+ = \begin{cases} x & x \ge 0 \\ 0 & \text{otherwise} \end{cases}. \qquad (6)$$

Note that the capacity is achieved by precoding the two data streams with the right singular vectors of $\boldsymbol{H}$, denoted by $[\boldsymbol{v}_1 \ \boldsymbol{v}_2]$:

$$\boldsymbol{H} = [\boldsymbol{u}_1 \ \boldsymbol{u}_2]\begin{bmatrix} \sqrt{\lambda_1} & 0 \\ 0 & \sqrt{\lambda_2} \end{bmatrix}[\boldsymbol{v}_1 \ \boldsymbol{v}_2]^H. \qquad (7)$$

In particular, when $\boldsymbol{H}$ is rank-deficient, i.e. $\lambda_2 \simeq 0$, the water-filling power allocation performed in eq. (5) will assign all available transmission power to one data stream. As a result, the UT will effectively choose $\boldsymbol{v}_1$ as the rank-one beamforming PMI.

C. Impact of XPD

To investigate the impact on the MIMO channel capacity due to XPD, discussions on some particular structures of $\boldsymbol{H}$ are provided in this section. For illustration purposes, we assume perfect cross-polarization isolation and zero cross-antenna correlation. Finally, it should be emphasized that we model each entry of $\boldsymbol{H}$ as a zero-mean complex Gaussian random variable, which implicitly assumes NLOS environments.

1) High XPD:
V-V or H-H Transmit Antennas: We first consider the case in which both chosen TX antennas have the same polarization. Using V-V TX antennas as an example, the corresponding $\boldsymbol{H}$ can be modeled as

$$\boldsymbol{H}_{VV} = \begin{bmatrix} \mathcal{CN}\left(0, \frac{\gamma}{1+\gamma}\right) & \mathcal{CN}\left(0, \frac{\gamma}{1+\gamma}\right) \\ \mathcal{CN}\left(0, \frac{1}{1+\gamma}\right) & \mathcal{CN}\left(0, \frac{1}{1+\gamma}\right) \end{bmatrix}, \qquad (8)$$

where $\mathcal{CN}\left(\alpha, \sigma^2\right)$ is the complex Gaussian distribution with mean α and variance σ^2, and γ denotes the XPD. Now, if XPD is sufficiently large, i.e. $\gamma \to \infty$, then $\boldsymbol{H}_{VV}$ becomes

$$\boldsymbol{H}_{VV,\gamma\to\infty} = \begin{bmatrix} \mathcal{CN}(0,1) & \mathcal{CN}(0,1) \\ 0 & 0 \end{bmatrix}. \qquad (9)$$

Inspection of eq. (9) suggests that the resulting MIMO channel is rank-deficient, which is favorable for beamforming particularly in the low SNR regime.
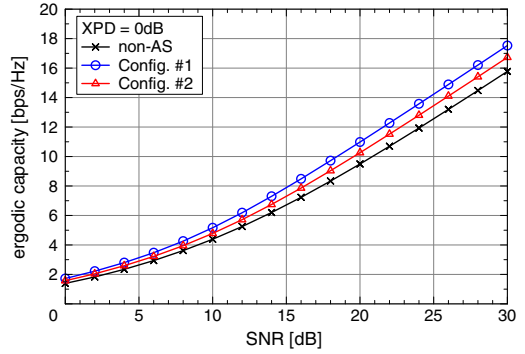

Fig. 6. Ergodic capacity vs. SNR using 2, 3 and 4 antennas at XPD of $\gamma = 0$ dB.

V-H Transmit Antennas: We next consider the case of one pair of vertically and horizontally polarized TX antennas. Then, the corresponding $\boldsymbol{H}$ can be modeled as

$$\boldsymbol{H}_{VH} = \begin{bmatrix} \mathcal{CN}\left(0, \frac{\gamma}{1+\gamma}\right) & \mathcal{CN}\left(0, \frac{1}{1+\gamma}\right) \\ \mathcal{CN}\left(0, \frac{1}{1+\gamma}\right) & \mathcal{CN}\left(0, \frac{\gamma}{1+\gamma}\right) \end{bmatrix}. \qquad (10)$$

If XPD is sufficiently large i.e. $\gamma \to \infty$, then $\boldsymbol{H}_{VH}$ becomes

$$\boldsymbol{H}_{VH,\gamma\to\infty} = \begin{bmatrix} \mathcal{CN}(0,1) & 0 \\ 0 & \mathcal{CN}(0,1) \end{bmatrix}. \qquad (11)$$

Equation (11) reveals that $\boldsymbol{H}_{VH,\gamma\to\infty}$ is comprised of two equal-power independent sub-channels, which is particularly favorable for multiplexing in the high SNR regime.

2) Low XPD: Finally, if XPD is rather small, i.e. $\gamma \to 1$, then $\boldsymbol{H}$ becomes

$$\boldsymbol{H}_{\gamma\to 1} = \begin{bmatrix} \mathcal{CN}(0,1/2) & \mathcal{CN}(0,1/2) \\ \mathcal{CN}(0,1/2) & \mathcal{CN}(0,1/2) \end{bmatrix}. \qquad (12)$$

As a result, it becomes equally probable for all antenna combinations to be chosen. Note that MIMO channels with UT's cross-polarized antennas of a 45-degree slanted angle can be equivalently modeled as eq. (12).

IV. SIMULATION RESULTS

In this section, simulation results are shown to compare the achievable capacity obtained with two cross-polarized antennas as well as antenna selection via choosing two antennas as shown in Fig. 5. Note that we assume ideal precoding in the following evaluation for the sake of simplicity.

A. Evaluation over Rayleigh Fading

For a fundamental study, we first examine the basic performance over frequency-nonselective Rayleigh fading channels instead of established models.

Figure 6 shows the ergodic capacity obtained at XPD of $\gamma = 0$ dB. The baseline system is non-AS (fixed to 1H-2V as shown in Table II). Inspection of Fig. 6 shows that Configurations #1 and #2 outperform non-AS by about 2 and 1 bps/Hz at high SNR, respectively. This observation matches well with the analytical results reported in the literature [6], [7]. At an ergodic capacity of 10 bps/Hz, Configurations #1 and #2 provide about 2.5 dB and 1.5 dB gains as compared to the non-AS, respectively.

Next, we show the percentage of capacity increase of Configurations #1 and #2 as compared to the non-AS. For $\gamma = 0$ dB, Fig. 7 shows that Configuration #2 provides about 10% over the SNR range of 0–30 dB whereas Configuration #1 has more impressive performance at low SNR regime (about 20%) and
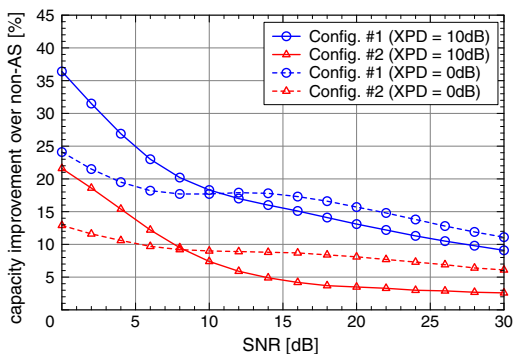
Fig. 7. Capacity improvement vs. SNR at XPD of $\gamma = 0$ dB and 10 dB.
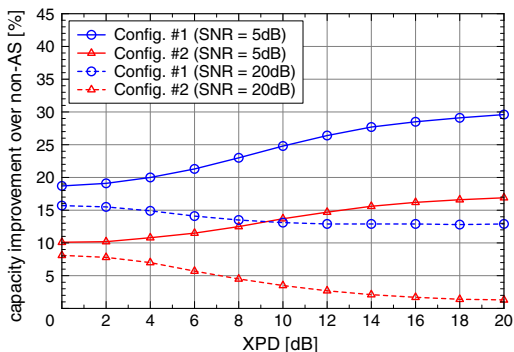

Fig. 8. Capacity improvement vs. XPD at SNR of $\rho = 5$ dB and 20 dB.

Fig. 9. Percentage of capacity increases over non-AS in Configuration #1.

decreasing gain in the high SNR regime. Interestingly, for $\gamma = 10$ dB, Configurations #1 and #2 have more significant gains in the low SNR regime. This is because the beamforming gain derived from V-V and H-H beamforming is more apparent in the low SNR and high XPD as discussed in Section III-C. On the other hand, the V-V and H-H antenna combinations at high XPD offer little advantages as compared to V-H combinations in the high SNR.

Figure 8 shows the percentage of capacity increase of Configurations #1 and #2 as compared to the non-AS as a function of XPD at SNR of $\rho = 5$ dB and 20 dB. At low SNR, the performance gains derived from Configurations #1 and #2 increase with XPD. In contrast, at SNR of $\rho = 20$ dB, the antenna selection performance is less sensitive to XPD. This is because the MIMO channel matrix using V-V and H-H combinations becomes rank-deficient at high XPD and, subsequently is less likely to be selected in the high SNR regime.

B. Evaluation over the Developed Channel Model

In this section, we evaluate the antenna selection performance using our channel model. Here we discuss the results obtained by the Scenario B model, namely an office NLOS environment with XPD of $\gamma = 0.3$ dB. We assume that the BS sits at the origin in the *x-y* coordinate system and compute the ergodic capacity across a 1m × 1m grid over a 20m × 20m area. At each grid point, 200 random samples are generated. Furthermore, we set the TX power of the BS and noise floor level at 10 dBm and −90 dBm, respectively. We simulate a system of 5 MHz bandwidth with 512 subcarriers.

The percentage of capacity increase with antenna selection is shown in Fig. 9. Note that we show the performance for Configuration #1 only due to limitations of space. We found that the improvement with antenna selection is significant near
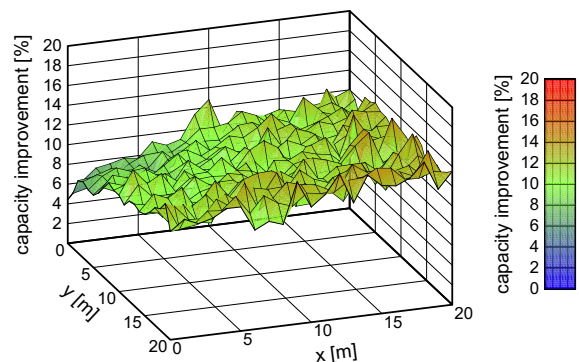
the edges (up to 13%) in the shown area, where SNR is about 20–25 dB. Note that diversity gains yielded by antenna selection significantly appear in low cumulative frequencies when evaluating cumulative distribution of the instantaneous capacity. We also confirmed up to 7% improvement in Configuration #2 although its performance is omitted. Considering the SNR and XPD, the result is consistent with the discussion in Section IV-A. It is expected that a cross-polarized antenna selection technique yields benefits especially for cell-edge users.

V. Conclusions

In this paper, we have presented the MIMO polarized channel models developed in our recent measurement campaigns. We have confirmed the validity of the newly developed models via comparison with the existing WINNER models. Furthermore, we have evaluated the ergodic capacity performance using cross-polarized antenna selection. It has been shown that systems selecting two antennas from 4 antennas and 3 antennas harvest about 2 and 1 bps/Hz improvement in the high SNR regime as compared to those without antenna selection, respectively. Finally, it has been shown that antenna selection is particularly useful in the low SNR regime. Using one of the developed channel models, simulation results suggested that selecting two antennas from 4 antennas and 3 antennas can increase the system capacity by about 13% and 7% near the edges of a 20m × 20m area, respectively.

References

[1] IST-4-027756 WINNER II, D1.1.2 V1.2, "WINNER II channel models," Sept. 2007.

[2] S. Kozono, T. Tsuruhara, and M. Sakamoto, "Base station polarization diversity reception for mobile radio," IEEE Trans. Veh. Technol., vol.33, no.4, pp.301–306, Nov. 1984.

[3] O.L. Frost, III, "An algorithm for linearly constrained adaptive array processing," Proc. IEEE, vol.60, no.8, pp.926–935, Aug. 1972.

[4] R.M. Författare, J.-E. Berg, F. Harrysson and H.T. Asplund, "Carrier frequency effects on path loss," in Proc. VTC2006-Spring, pp.2717–2721, May 2006.

[5] 3GPP TS 36.211 V.9.1.0, "3rd generation partnership project: technical specification group radio access network; evolved universal terrestrial radio access (E-UTRA); Physical Channel and Modulation," March 2010.

[6] S. Sanayei and A. Nosratinia, "Capacity of MIMO channels with antenna selection," IEEE Trans. Inf. Theory, vol.53, no.11, pp.4356–4362, Nov. 2007.

[7] A. Molisch, M.Z. Win, Y.-S. Choi and J. Winters, "Capacity of MIMO systems with antenna selection," IEEE Trans. Wireless Commun., vol.4, no.4, pp.1759–1772, July 2005.